coatings

MDPI

Article

Fabrication of MnCoS Thin Films Deposited by the SILAR Method with the Assistance of Surfactants and Supercapacitor Properties

Qifan Yang [1], Qianhui Chen [1], Fuzhong Gong [1,2,*] and Yanlin Li [1,2]

[1] School of Chemistry and Chemical Engineering, Guangxi University, Nanning 530004, China
[2] Guangxi Key Laboratory of Petrochemical Resource Processing and Process Intensification Technology, Nanning 530004, China
* Correspondence: fzgong@gxu.edu.cn

Abstract: Compact MnCoS thin films on a nickel foam (NF) substrate were prepared by successive ionic layer adsorption and a reaction (SILAR) method, and two surfactants (SDS and CTAB) were used to improve the wettability of the NF. The MnCoS thin films were characterized by scanning electron microscopy (SEM), transmission electron microscopy (TEM), X-ray diffraction (XRD), and X-ray photoelectron spectroscopy (XPS). The supercapacitive properties were evaluated by cyclic voltammetry (CV), galvanostatic charge–discharge (GCD), and impedance spectroscopy (EIS). The results show that while the NF was first dipped in surfactant solution, followed by a mixture of Mn^{2+} and Co^{2+} or a Na_2S solution, the load and density of the MnCoS on the NF's surface significantly increased and delivered a much higher specific capacitance than that of the MnCoS thin film formed without the assistance of surfactants, which were 2029.8 F g^{-1} (MnCoS-CTAB), 1500.3 F g^{-1} (MnCoS-SDS), and 950.4 F g^{-1} (MnCoS-H_2O) at a current density of 1 A g^{-1} in 3 M KOH aqueous solution. When the current density increased to 10 A g^{-1}, the MnCoS-CTAB with the highest specific capacitance exhibited a capacitance of 1371.9 F g^{-1}, with a 71% capacity retention up to 1000 cycles, showing a good rate performance and cycle stability.

Keywords: MnCoS; thin film; SILAR method; surfactant; supercapacitor

check for updates

Citation: Yang, Q.; Chen, Q.; Gong, F.; Li, Y. Fabrication of MnCoS Thin Films Deposited by the SILAR Method with the Assistance of Surfactants and Supercapacitor Properties. *Coatings* **2023**, *13*, 908. https://doi.org/10.3390/coatings13050908

Academic Editor: Mojtaba Mirzaeian

Received: 31 December 2022
Revised: 8 April 2023
Accepted: 11 April 2023
Published: 11 May 2023

Copyright: © 2023 by the authors. Licensee MDPI, Basel, Switzerland. This article is an open access article distributed under the terms and conditions of the Creative Commons Attribution (CC BY) license (https://creativecommons.org/licenses/by/4.0/).

1. Introduction

Energy crises and ecological issues are common problems facing mankind today and are also the focus of researchers. It is very necessary to develop environmentally friendly, economical, and sustainable energy [1]. Photovoltaic power, wind energy, potential energy from water, hydrogen, and geothermal energy, etc., are representative of environmentally friendly energy. In the meantime, research on energy storage technology is equally necessary and urgent. At present, hydrogen production by water splitting and reversible charge–discharge electrochemical devices are the most advanced energy storage technology, and the latter includes charge–discharge batteries, such as lithium ion batteries and sodium ion batteries, and supercapacitors [2–4].

Supercapacitors were developed in the 1980s. They use electrochemical components that polarize electrolytes to store energy without chemical reactions, and they have the unique properties of ecofriendliness, high power density, quick charge–discharge rate, good cycling stability, and long cycle life [4]. Supercapacitors can be divided into three categories: electrical double-layer capacitors (EDLCs), pseudocapacitors (Faradaic supercapacitors), and hybrid supercapacitors. In EDLCs, the capacitance generates from the charge accumulation at the electrode interface, and the main active materials applied in EDLCs are carbon materials with a high surface area, such as activated carbon, graphene, and carbon nanotubes [5,6]. In pseudocapacitors, the capacitance is primarily derived from the reversible redox reaction of the active material and, thus, exhibits higher capacitance and

energy values compared to EDLCs [7]. The active materials include transition metal oxides (TMOs), transition metal sulfides (TMSs), transition metal hydroxides, and conductive polymers [7–10]. A hybrid capacitor is a combination of an EDLC and a pseudocapacitor.

TMSs have gained extensive interest in energy storage devices lately owing to their low cost and unique features, such as high specific capacity, better reactivity and conductivity, and low electronegativity of the sulfur elements [1,2,11,12]. Moreover, many studies have confirmed that binary metal sulfides exhibit better electrochemical performance than monometallic sulfide, mainly due to the fact of their high electronic conductivity, multiple oxidation states, and cooperative redox reaction [13–20]. Sangeetha et al. fabricated CoS/MoS material grown on activated carbon fiber using a one-step hydrothermal method, which had a specific capacitance of 733 F g^{-1} at a current density of 0.5 A g^{-1} [18]. The MnS/Ni_xS_y materials prepared by Pan et al. via a hydrothermal method provided a high specific capacitance of 1073.81 F g^{-1} at a current density of 1 A g^{-1} [19]. The NiS/CoS core–shell nanosheet composites prepared by Miao et al. via hydrothermal and electrodeposition methods on nickel foam showed a specific capacitance of up to 1210 F g^{-1} at a current density of 1 A g^{-1} [20].

Among the TMSs, manganese–cobalt sulfides have a high specific capacity owing to their multiple oxidation states, which are conducive to Faraday redox reactions, and the natural abundance of manganese resources. However, due to the high dependence of the redox reaction, the diffusion rate, capacity, and electrochemical stability of the manganese–cobalt sulfides in a rapid charge and discharge process are not ideal. In addition, the serious accumulation of manganese–cobalt sulfide particles will reduce the electron transfer and ion diffusion [21–25]. To solve these problems, different structures of manganese–cobalt sulfides have been fabricated, such as nanospheres [22], nanotubes [23], nanoflowers [24,25], nanowires [26], and nanosheets [27]. The prepared methods involve liquid deposition, vapor deposition, electrodeposition, and hydrothermal methods. The first two methods require complex vacuum equipment, and the latter is difficult to achieve for large-scale production.

SILAR is a simple and cheap method for depositing semiconductor materials on various substrates. It does not require a vacuum system, complex equipment, or adhesives. A dense thin film of active materials is vital for the electrochemical performance of a supercapacitor, and the deposition of a dense thin film using the SILAR method on a substrate without a binder is still challenging due to the small surface area and poor wettability of the substrate's surface [28–36].

Surfactants are substances with an amphiphilic group, that is, one hydrophilic group and one hydrophobic group in their molecule structure. They can improve the wettability of a solid surface by reducing the surface tension of the solution. In this paper, two surfactants were used in the preparation of binary metal sulfide (MnCoS) thin film electrodes using the SILAR method. $Mn(CH_3COO)_2$, $Co(NO_3)_2$, and Na_2S were used as reactants and foam nickel as the substrate. One surfactant was SDS (sodium dodecyl sulfate), which was anionic. The other was CTAB (cetyl trimethyl ammonium bromide), which was cationic. With the help of the surfactant, the load of MnCoS greatly increased and formed dense deposited MnCoS thin films. The capacity also significantly increased, and they exhibited an excellent electrochemical performance.

2. Experimental

2.1. Materials

Sodium sulfide nonahydrate ($Na_2S{\cdot}9H_2O$), manganese acetate tetrahydrate [$Mn(CH_3COO)_2{\cdot}4H_2O$], cobalt nitrate hexahydrate [$Co(NO_3)_2{\cdot}6H_2O$], potassium hydroxide (KOH), cetyl trimethyl ammonium bromide (CTAB), and sodium dodecyl sulfonate (SDS) were purchased from Macklin Reagent Co., Ltd., Shanghai, China Nickel foam (NF), platinum electrodes, and Hg/HgO electrodes were purchased from Kelude Co., Ltd., Shenzhen, China. The aqueous solutions of 25 mL 0.1% SDS, 25 mL 0.1 M Na_2S, and 25 mL

0.1 M Mn^{2+} and Co^{2+} were prepared in advance. DI water with a measured resistivity of 18 MΩ·cm was used in all experiments.

2.2. Deposition of MnCoS Thin Films

In the SILAR experiment, the NF was first immersed in surfactant solution through the electrostatic interaction between the charged groups of the surfactant adsorbed on substrate and positive (or negative) ions. The adsorption of metal ions on the substrate's surface improved and, finally, the loading of binary metal sulfide (MnCoS) increased. Meanwhile, a dense thin film of MnCoS deposited on the nickel foam's surface formed. NF of a size of 2 cm × 1 cm was cleaned well with DI water and dried before use as the substrate. A MnCoS thin film electrode was prepared according to the follow process: (1) the dried NF was initially dipped in 25 mL 0.1%SDS solution for 30 s to adsorb SDS over the NF substrate and cause the surface of the substrate to have a negative charge; (2) the substrate was immersed for 30 s in DI water to eliminate the excess adsorbed and loosely bonded SDS; (3) the substrate was dipped in mixed aqueous solution containing both Mn^{2+} and Co^{2+} for 30 s, which were adsorbed on the substrate's surface by electrostatic interaction with SDS; (4) the substrate was immersed for 30 s in DI water again; (5) the substrate was dipped in Na_2S solution, where the S^{2-} ions reacted on the pre-adsorbed Mn^{2+} and Co^{2+} ions; and (6) the substrate was again immersed for 30 s in DI water to eliminate the unreacted S^{2-} ions or weakly bound MnCoS composite. After repeating 10 SILAR cycles, the MnCoS thin film electrode was obtained and named as MnCoS-SDS. Likewise, the MnCoS-CTAB thin films were prepared like that of the MnCoS-SDS with CTAB instead of SDS. The difference is that because CTAB is a cationic surfactant, it was first dipped in the Na_2S solution to absorb S^{2-} ions and then dipped in the mixed solution of Mn^{2+} and Co^{2+} to absorb cations. For comparison, the MnCoS-H_2O electrode was also fabricated for a case without the assistance of a surfactant. All prepared electrodes were dried at 60 °C overnight before being used for the subsequent electrochemical measurements. The mass loading of the active material MnCoS on the NF was determined by monitoring the mass difference of the NF electrodes before and after the modification, which were 0.9 ± 0.1 mg/cm^2, 0.8 ± 0.1 mg/cm^2, 0.5 ± 0.1 mg/cm^2 for the MnCoS-SDS, MnCoS-CTAB, and MnCoS-H_2O electrodes, respectively. The loading of MnCoS increased obviously by 1.6 times after the pretreatment with the surfactant solution. The SILAR experimental process for the deposition of the MnCoS thin films is shown in Figure 1.

2.3. Characterizations

The surface morphology of the deposited thin film was observed using field emission scanning electron microscopy (FESEM) with energy-dispersive X-ray spectroscopy (EDS) analysis equipment (Regulus8100, Toyko, Japan) and a high-resolution transmission electron microscope (HR–TEM, FEI Tecnai G2 F20). The phase crystallinity was analyzed by an X-ray diffractometer (Rigaku D/Max-2500V, Tokyo, Japan) with Cu-Kα radiation (λ = 1.54056 Å) in the 2θ range of 10°–80°. X-ray photoelectron spectroscopy (XPS) analysis was conducted using the Mg Kα line (SPECS, Kleve, Germany, XR50 and 200 W) at 1253 eV and a Phoibos 100 spectrometer. The survey scan and high-resolution Mn 2p, S 2p, and Co 2p were recorded using an electrodeposited SP electrode, which was attached to the sample holder by carbon tape. The adventitious carbon 1 s at 284.5 eV was used for the calibration.

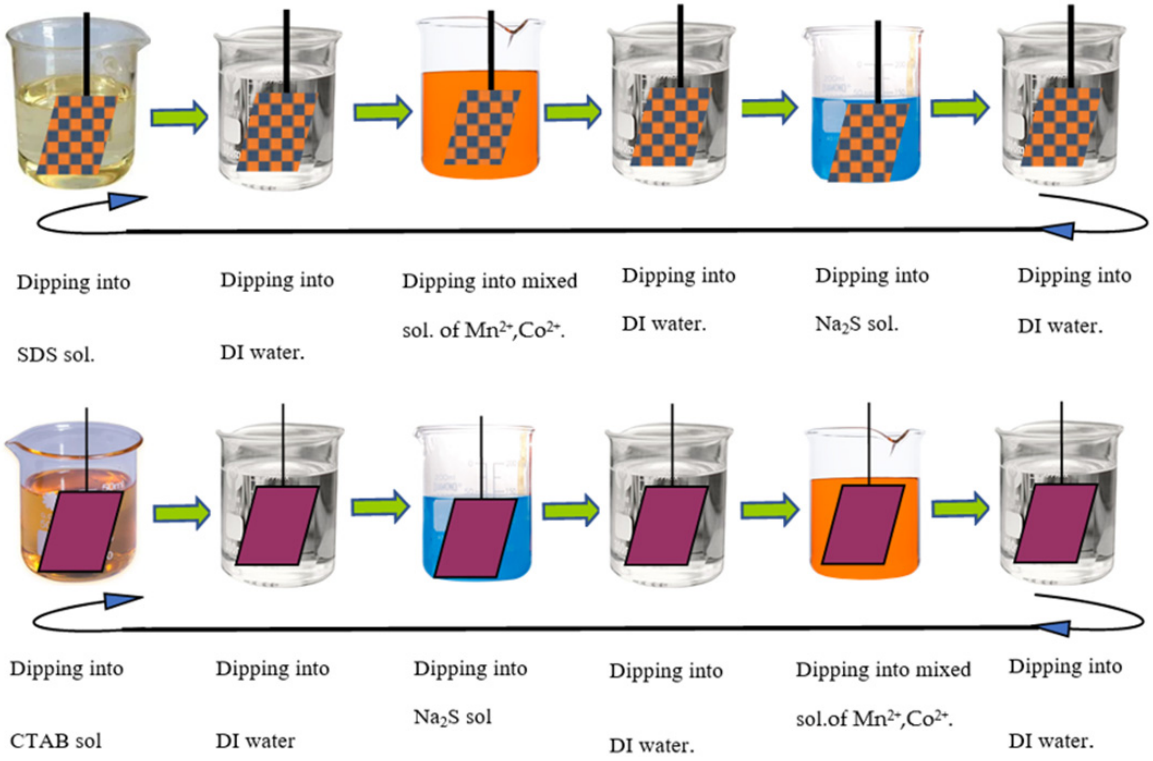


Figure 1. Flowchart of the MnCoS thin films prepared using the SILAR method.

2.4. Electrochemical Measurements

The electrochemical properties of the as-prepared active materials were studied using a CS350 electrochemical workstation (Wuhan Koster Instrument Co., Ltd., Wuhan, China) with a three-electrode system. The nickel foam, platinum, Hg/HgO electrode, and 3 M KOH were used as the working electrode, opposite electrode, reference electrode, and electrolyte, respectively. The cyclic voltammetry (CV), galvanostatic charge–discharge (GCD), and electrochemical impedance spectroscopy (EIS) tests were used to characterize the electrochemical behavior of the supercapacitor. The specific capacitance was obtained based on the charge–discharge curve, and the formula for its calculation is as follows [37,38]:

$$C_m = I\,\Delta t / m\,\Delta V \quad (1)$$

where C_m is the specific capacity of the supercapacitor, Δt is the discharge time, I is the discharge current, ΔV is the potential window, and m is the total mass of the active substance on the working electrode.

3. Results and Discussion

3.1. Characterization

Figure 2 shows the morphologies of the deposited thin films of MnCoS-H_2O, MnCoS-SDS, and MnCoS-CTAB. For the MnCoS-H_2O sample, as shown in Figure 2a, there was a part of the nickel foam surface that was not covered by MnCoS particles, and the particles deposited in the covered part were grouped together in a form similar to islands. For the MnCoS-SDS electrode, as shown in Figure 2b, the surface of the nickel foam was almost completely covered by a thick layer of $MnCoS_x$ particles, but several cracks were observed. With regard to the MnCoS-CTAB electrode, the surface of the nickel foam was completely covered by a layer of $MnCoS_x$ particles, and only a few small cracks appeared, as shown in Figure 2c, indicating that a thick and dense coating formed. This confirms that the pretreatment of the nickel foam by surfactant is very beneficial to the deposition of particles on the surface. The EDS analysis, shown in Figure 2d–f, reveals that the three elements

of Mn, Co, and S in MnCoS-CTAB has an evenly distributed state. It is well known that the surfactants of SDS and CTAB are substances with an amphiphilic group, that is, one hydrophilic group and one hydrophobic group in their molecule structure, which are shown as $CH_3(CH_2)_{10}CH_2$-OSO_3Na(SDS) and $CH_3(CH_2)_{14}CH_2$-$N^+(CH_3)_3Br$ (CTAB), where the hydrophobic group refers to $CH_3(CH_2)_{10}CH_2$- for SDS and $CH_3(CH_2)_{14}CH_2$- for CTAB. The hydrophilic group refers to -$N^+(CH_3)_3$ and -OSO_3^-, which had a positive charge and negative charge, respectively. The hydrophobic group is a carbon chain. The surfactants are easily adsorbed onto the surface of the nickel foam spontaneously to decrease the surface free energy, changing the wetting properties and electrical properties of the surface. Through the electrostatic interaction between the charged ionic groups of the surfactant and MnCoS nanoparticles, the mass of the particles deposited on the surface of the nickel foam increased significantly and formed a dense film. The TEM images of the MnCoS-CTAB composite, shown in Figure 2g, further confirms the compact structure of the MnCoS thin film, which consisted of nanoparticles with a size of ~20 nm. The lattice fringes of 0.276 and 0.305 nm identified in the HRTEM image (Figure 2h) corresponded to the CoS (200) and MnS (200) lanes, respectively [39].

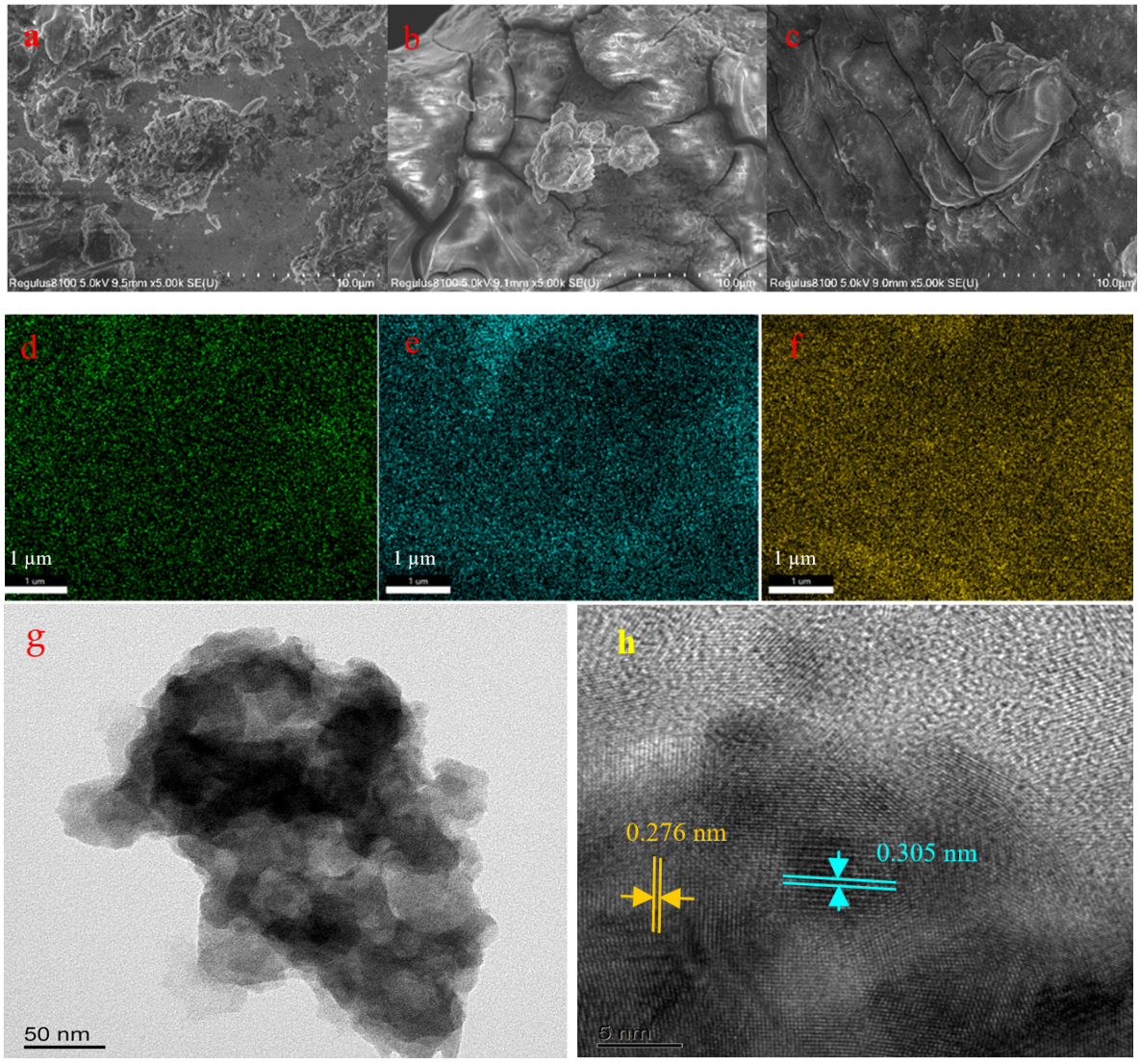


Figure 2. SEM images: (**a**) MnCoS; (**b**) MnCoS-SDS; (**c**) MnCoS-CTAB. EDS patterns: (**d**) S; (**e**) Mn; (**f**) Co of the MnCoS-CTAB composite. TEM images (**g**) and HRTEM image (**h**) of MnCoS-CTAB.

Figure 3 shows the XRD patterns of the MnCoS-H_2O, MnCoS-SDS, and MnCoS-CTAB. The three peaks at the diffraction angles of 44.5°, 51.8°, and 76.4° in the XRD pattern were caused by the nickel foam, corresponding to the (111), (200), and (220) crystal planes of Ni (JCPDS 87-0712). However, in addition to the diffraction peaks of the nickel foam, only MnCoS-CTAB and MnCoS-SDS showed a weak diffraction peak at 21°, which did not appear in the MnCoS-H_2O; this is because the amount of active material loaded on the surface of the nickel foam was too small, leading to the failure of their detection by XRD.

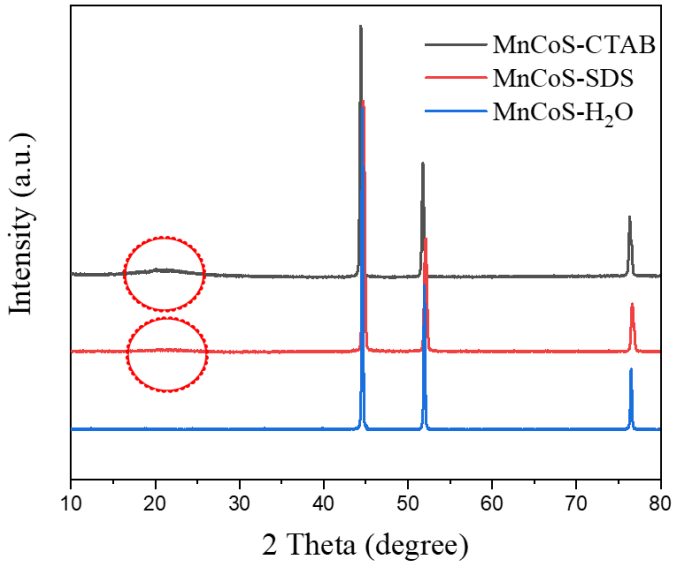


Figure 3. XRD patterns of the MnCoS film loaded on the surface of the nickel foam.

The chemical element composition and the valence state of the MnCoS-CTAB materials were analyzed by XPS. Figure 4a is the XPS spectrum of the survey scanning, indicating that the Co, Mn, S, Ni, and O elements were detected; the appearance of oxygen arose due to the oxidation of the MnCoS-CTAB sample after exposure to the air; and the Ni element was inevitably detected from the nickel foam. In the high-resolution spectrum of Mn 2p (Figure 4b), it was observed that the Mn 2p peak at a binding energy of 642.5 eV was attributed to Mn $2p_{3/2}$ [22,23], and no other peaks appeared, indicating that the Mn element existed only in the form of Mn^{2+}. Figure 4c shows that the Co 2p peak consisted of two spin-orbit splitting peaks and two restructured satellites peaks, and the peaks at a binding energy of 786.9 eV and 802.4 eV belonged to Co^{2+}, and the peaks at 781.3 eV and 797.3 eV corresponded to Co^{3+} [25,26], indicating that the Co existed in the form of Co^{2+} and Co^{3+}, of which Co^{2+} was the main one. The coexistence of the mixed valence states of Co provided a variety of redox reaction types, which contributed to the excellent electrochemical performance. Figure 4d indicates that the S 2p peak contained two peaks at binding energy peaks of 162.9 eV and168.6 eV, the peak at 162.9 eV was consistent with MnS and CoS, and the satellite peak of sulfide was observed at 168.8 eV [27,38].

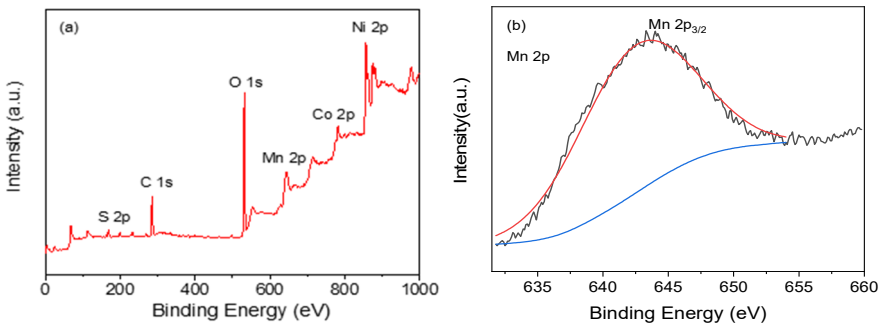


Figure 4. *Cont.*

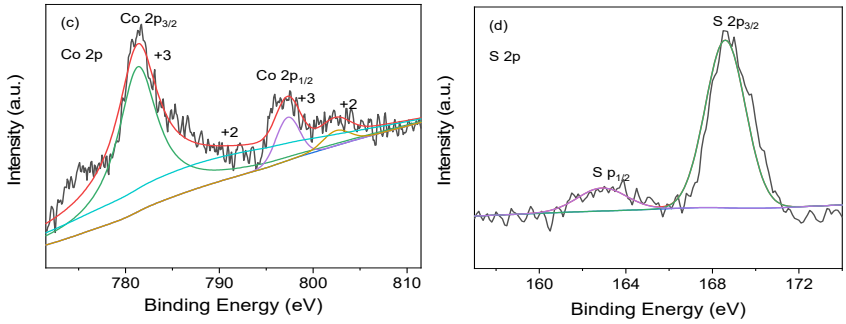


Figure 4. (**a**) XPS spectra of the survey scan and high-resolution spectrum of (**b**) Mn 2p; (**c**) Co 2p; (**d**) S 2p. The spectra were calibrated to the C 1 s peaks at 284.5 eV.

3.2. Electrochemical Performance

Figure 5a shows the CV curves of MnCoS-H_2O, MnCoS-SDS, and MnCoS-CTAB in a potential window of 0–0.5 V at a scanning rate of 5 mV s^{-1}. As shown, the prominent oxidation and reduction peaks indicate the pseudo-like capacitive behavior of the electrode; moreover, the integral area of MnCoS-SDS and MnCoS-CTAB was obviously larger than that of MnCoS-H_2O, which verifies that the formation of a compact thin film on the surface of the nickel substrate can remarkably improve the electrochemical performance of the MnCoS active material. The CV curves of MnCoS-CTAB, shown in Figure 5b, indicated that with the increase in the scanning rate, the potential of the cathode peaks decreased, and the potential of the anode peaks increased, indicating that the polarization degree of the active material increased, but the CV curve had no obvious distortion at the different scanning rates, showing that the membrane of the MnCoS-CTAB active material had good stability. The GCD results shown in Figure 5c revealed that the charge–discharge curves displayed an obvious plateau at ~0.3 V, which corresponds to the potential of the redox peaks in the CV curves, illustrating the occurrence of a Faraday reaction. It can also be seen from Figure 5c that the MnCoS-CTAB delivered the highest specific capacity of 2029.8 F g^{-1}, higher than that of MnCoS-SDS (1500.2 F g^{-1}) and MnCoS-H_2O (950.4 F g^{-1}). The resistive and capacitive behaviors of the MnCoS-H_2O, MnCoS-SDS, and MnCoS-CTAB electrodes were studied using electrochemical impedance spectroscopy (EIS) in the frequency range of 100 kHz to 0.01 Hz. A Nyquist plot is shown in Figure 5d, and the inset is the equivalent circuit fitted to the Nyquist plot, where Rs is the bulk solution resistance, which is the sum of the internal resistance of the electrode and the resistance of the electrolyte, C_d is the double layer capacitance, R_{ct} and Z_w are the charge transfer resistance and the diffusion resistance or the Warburg impedance, respectively. Both of them occurred one after the other, which makes them a series [38]. It is clearly observed that the three curves were composed of small but inconspicuous semicircles in the high-frequency region and straight lines in the low-frequency region. Obviously, the MnCoS-CTAB electrode displayed the smallest semicircle diameter and the highest straight line slope, implying that it had the smallest internal resistance, charge transfer resistance, and Warburg resistance. The order of the three resistances was as follows: MnCoS-CTAB > MnCoS-SDS > MnCoS-H_2O. The lower resistances are beneficial for the fast electron transfer and ion diffusion through electrode materials. This further explains why MnCoS-CTAB possessed the highest specific capacitance and the best rate capability.

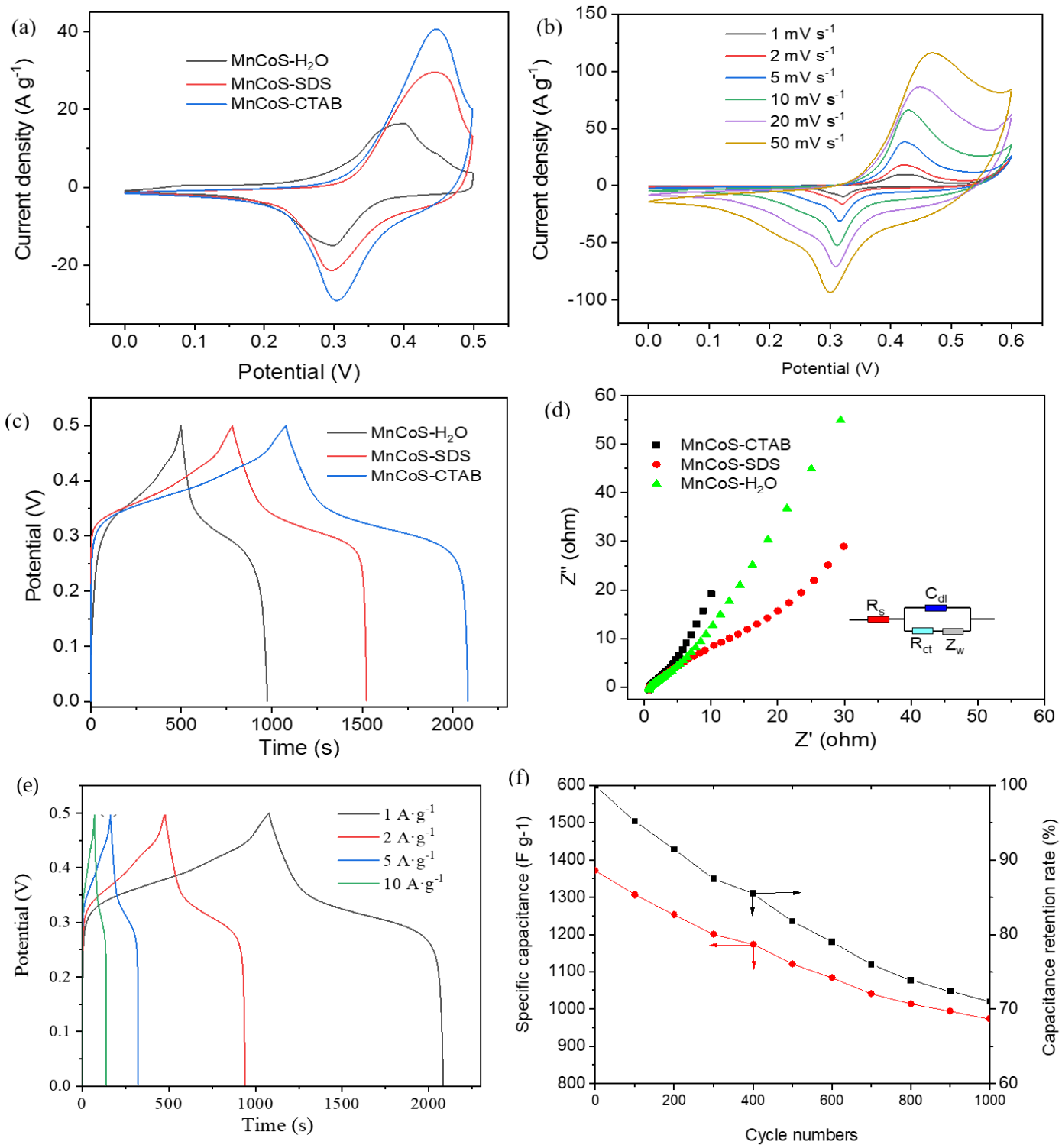


Figure 5. (**a**) CV profile at 5 mV s^{-1}; (**b**) CV profile at various scan rates; (**c**) GCD curves at 1 A g^{-1}; (**d**) Nyquist plot; (**e**) GCD curves at different current densities; (**f**) specific capacitance (red line) and retention rate (black line) at different cycles of the MnCoS-CTAB electrode.

The electrochemical performance of MnCoS-CTAB was further studied by GCD tests at different current densities ranging from 1 to 10 A g^{-1} at the potential window of 0–0.5 V. As shown in Figure 5e, the potential platform in the charge–discharge curve represents the ideal behavior of the battery-type supercapacitor. The charge–discharge curves at the different current densities had approximate symmetry, indicating the small energy loss,

good coulomb efficiency, and reversible redox reaction in the charge–discharge process. The specific capacitances calculated by the discharge time at the current densities of 1, 2, 5, and 10 A g^{-1} were 2029.8, 1850.2, 1604.1, and 1371.9 F g^{-1}, respectively, indicating that both the discharge time and the specific capacitance of MnCoS-CTAB decreased with the increase in the current density. Moreover, the cyclic stability performance test was carried out at a current density of 10 A g^{-1}, as shown in Figure 5f, and the specific capacity of MnCoS-CTAB remained at 974.0 F g^{-1} after 1000 cycles, with a capacity retention rate of 71%, showing that MnCoS-CTAB had long-term cyclic stability.

For comparison, the specific capacity of other transition metal sulfides prepared using the hydrothermal method and SILAR method are listed in Table 1. It is clearly indicated that the MnCoS-CTAB electrode prepared in this work displayed a high specific capacity, higher than that of the monometal sulfides thin film synthesized by SILAR and binary metal sulfides synthesized by the hydrothermal method, in general, but lower than that binary metal sulfides synthesized by electrodeposited method. This may be the reason that a denser and stronger thin film was formed by the electrodeposited method, because the electrodeposition is driven by the external electric field, and the charged particles can be deposited quickly and evenly on the electrode surface.

Table 1. Comparison of the specific capacity of transition metal sulfides.

Electrodes	Synthesis Method	Specific Capacity	Reference
CoS/MoS	hydrothermal	733 F g^{-1} at 0.5 A g^{-1}	[18]
MnS/NixSy	hydrothermal	1073.8 F g^{-1} at 1 A g^{-1}	[19]
NiS/CoS nanosheet	hydrothermal	1210 F g^{-1} at 1 A g^{-1}	[20]
$Co_{0.5}Mn_{0.5}S$	sonochemical approach	893.3 F g^{-1} at 1 A g^{-1}	[21]
$NiCo_2S_4$	micelle-confined growth	1304 F g^{-1} at 2 A g^{-1}	[40]
NiS_2-CoS_2	hydrothermal	954.3 F g^{-1} at 1 A g^{-1}	[41]
CuS/MnS composite	hydrothermal	1144 F g^{-1} at 1 A g^{-1}	[42]
$MnCo_2S_4$ core/shell	hydrothermal	2067 F g^{-1} at 1 A g^{-1}	[43]
CuMnS thin film	electrodeposited	1691 F g^{-1} at 10 A g^{-1}	[44]
CoMnS thin film	electrodeposited	2290 F g^{-1} at 10 A g^{-1}	
MnS thin film	SILAR	632 F g^{-1} at 0.2 A g^{-1}	[37]
NiCo(OH)(2)thin film	SILAR	1113 F g^{-1} at 1 A g^{-1}	[45]
Yb_2S_3 thin film	SILAR	181 F g^{-1} at 0.5 A g^{-1}	[46]
$NiCo_2S_4$	SILAR	1247 F g^{-1} at 1 A g^{-1}	[47]
Bi_2S_3 thin film	SILAR	289 F g^{-1} at 5 A g^{-1}	[48]
MnCoS-CTAB thin film	SILAR	2029.8 F·g^{-1} at 1 A g^{-1} 1371.9 F·g^{-1} at 10 A g^{-1}	This work

4. Conclusions

The MnCoS-CTAB and MnCoS-SDS electrodes were fabricated using the SILAR method with Na_2S, $Mn(CH_3COO)_2$, and $Co(NO_3)_2$ as reactants with the assistance of CTAB or SDS. By the adsorption of the surfactant on the surface of the nickel foam, the wettability and the charged properties of the nickel foam's surface changed. Through the electrostatic interaction between the charged ionic groups of the surfactant and the MnCoS nanoparticles, the loading of the particles deposited on the nickel foam surface increased significantly and formed a dense film, finally remarkably improving the specific capacity of the active material. The MnCoS-CTAB material showed the highest specific capacity of up to 2029.8 F g^{-1}, followed by MnCoS-SDS (1500.2 F g^{-1}), much higher than that of MnCoS-H_2O (950.4 F g^{-1}). The MnCoS-CTAB material also had a long-term cyclic stability with a retention rate of 71% of the specific capacity after 1000 cycles; thus, it showed good application prospects.

Author Contributions: Conceptualization, Q.Y. and F.G.; methodology, Q.Y.; software, Q.Y.; validation, Y.L. and F.G.; formal analysis, Q.Y.; investigation, Q.Y. and Q.C.; resources, F.G.; data curation, Q.Y. and Q.C.; writing—original draft preparation, Q.Y.; writing—review and editing, F.G.; visualization, Q.Y.; supervision, F.G.; project administration, Y.L.; funding acquisition, F.G. All authors have read and agreed to the published version of the manuscript.

Funding: This research received no funding.

Institutional Review Board Statement: Not applicable.

Informed Consent Statement: Not applicable.

Data Availability Statement: Not applicable.

Conflicts of Interest: The authors declare no conflict of interest.

References

1. Khan, M.T.N.; Ahmed, F.; Houda, S.; Manzoor, S.; Hasnain, K.; Zahra, M.; Hussain, R.; Ansari, M.Z.; Hegazy, H.H.; Ashiq, M.N. Facile synthesis of novel Ag@cerium zirconate heterostructure for efficient oxygen evolution reaction. *Surf. Interfaces* **2022**, *35*, 102410. [CrossRef]
2. Alburaih, H.A.; Ansari, M.Z.; Abid, A.G.; Khosa, R.Y.; Ashiq, M.N.; Manzoor, S.; Aman, S.; Chaudhry, H.; Waheed, M.S.; Taha, T.A. Study on active sites of Mn-doped iron selenide on pencil electrode for electrocatalytic water splitting. *J. Sol-Gel Sci. Technol.* **2022**, *22*, 05961. [CrossRef]
3. Owidah, Z.O.; Aman, S.; Abdullah, M.; Manzoor, S.; Fallatah, A.M.; Ibrahim, M.M.; Elnasr, T.A.; Ansari, M.Z. Metal oxide/carbon nanosheet arrays derivative of stacked metal organic frameworks for triggering oxygen evolution reaction. *Ceram. Int.* **2023**, *49*, 5936–5943. [CrossRef]
4. Theerthagiria, J.; Senthilc, R.A.; Nithyadharseni, P.; Lee, S.J.; Durai, G.; Kuppusami, P.; Madhavan, J.; Choi, M.Y. Recent progress and emerging challenges of transition metal sulfides based composite electrodes for electrochemical supercapacitive energy storage. *Ceram. Int.* **2020**, *46*, 14317–14345.
5. Kumar, S.; Saeed, G.; Zhu, L.; Hui, K.N.; Kim, N.H.; Lee, J.H. 0D to 3D carbon-based networks combined with pseudocapacitive electrode material for high energy density supercapacitor: A review. *Chem. Eng. J.* **2021**, *403*, 126352.
6. Wang, Y.F.; Zhang, L.; Hou, H.Q.; Xu, W.H.; Duan, G.G.; He, S.J.; Liu, K.M.; Jiang, S.H. Recent progress in carbon-based materials for supercapacitor electrodes: A review. *J. Mater. Sci.* **2021**, *56*, 173–200.
7. Abdah, M.A.A.M.; Azman, N.H.N.; Kulandaivalu, S.; Sulaiman, Y. Review of the use of transition-metal-oxide and conducting polymer-based fibres for high-performance supercapacitors. *Mater. Design* **2020**, *186*, 108199.
8. Ray, A.; Roy, A.; Saha, S.; Ghosh, M.; Chowdhury, S.R.; Maiyalagan, T.; Bhattacharya, S.K.; Das, S. Electrochemical Energy Storage Properties of Ni-Mn-Oxide Electrodes for Advance Asymmetric Supercapacitor Application. *Langmuir* **2019**, *35*, 8257–8267. [CrossRef]
9. Kandula, S.; RShrestha, K.; Kim, N.H.; Lee, J.H. Fabrication of a 3D Hierarchical Sandwich Co_9S_8/alpha-MnS@N-C@MoS_2 Nanowire Architectures as Advanced Electrode Material for High Performance Hybrid Supercapacitors. *Small* **2018**, *14*, e1800291. [CrossRef]
10. Zou, J.; Xie, D.; Zhao, F.; Wu, H.L.; Niu, Y.; Li, Z.J.; Zou, Q.M.; Deng, F.; Zhang, Q.; Zeng, X.R. Microwave rapid synthesis of nickel cobalt sulfides/CNTs composites as superior cycling ability electrode materials for supercapacitors. *J. Mater. Sci.* **2020**, *56*, 1561–1576.
11. Wang, Y.; Mayorga-Martinez, C.C.; Pumera, M. Polyaniline/MoS_X Supercapacitor by Electrodeposition. *Bull. Chem. Soc. Jpn.* **2017**, *90*, 847–853. [CrossRef]
12. Xin, B.; Zhao, Y.; Xu, C. A high mass loading electrode based on ultrathin Co_3S_4 nanosheets for high performance supercapacitor. *J. Solid State Electrochem.* **2016**, *20*, 2197–2205. [CrossRef]
13. Wu, F.M.; Gao, J.P.; Zhai, X.G.; Xie, M.H.; Gao, C.J.; Sun, Y.; Liu, Y.; Yan, J. Hierarchical zinc cobalt sulfide flowers grown on nickel foam as binder-free electrodes for high-performance asymmetric supercapacitors. *Electrochim. Acta* **2019**, *319*, 859–868. [CrossRef]
14. Zhang, G.H.; Xuan, H.C.; Wang, R.; Guan, Y.Y.; Li, H.S.; Liang, X.H.; Han, P.D.; Wu, Y.C. Enhanced supercapacitive performance in Ni_3S_2/MnS composites via an ion-exchange process for supercapacitor applications. *Electrochim. Acta* **2020**, *353*, 136517.
15. Yu, X.Y.; David, L.; Xu, W. Mixed metal sulfides for electrochemical energy storage and conversion. *Adv. Energy Mater.* **2018**, *8*, 1701592.
16. Yang, Q.; Liu, Y.; Yan, M.; Lei, Y.; Shi, W.D. MOF-derived hierarchical nanosheet arrays constructed by interconnected NiCo-alloy@NiCo-sulfide core-shell nanoparticles for high-performance asymmetric supercapacitors. *Chem. Eng. J.* **2019**, *370*, 666–676.
17. Chen, Y.X.; Jing, C.; Fu, X.; Shen, M.; Li, K.L.; Li, K.L.; Liu, X.Y.; Yao, H.C.; Zhang, Y.X.; Yao, K.X. Synthesis of porous NiCoS nanosheets with Al leaching on ordered mesoporous carbon for high-performance supercapacitors. *Chem. Eng. J.* **2020**, *384*, 123367.
18. Sangeetha, D.N.; Bhat, D.K.; Kumar, S.S.; Selvakumar, M. Improving hydrogen evolution reaction and capacitive properties on CoS/MoS_2 decorated carbon fibers. *Int. J. Hydrogen Energy* **2020**, *45*, 7788–7800.

19. Pan, Q.; Yang, X.; Yang, X.; Duan, L.F.; Zhao, L.J. Synthesis of a MnS/NixSy composite with nanoparticles coated on hexagonal sheet structures as an advanced electrode material for asymmetric supercapacitors. *Rsc. Adv.* **2018**, *8*, 17754–17763.
20. Miao, Y.; Zhang, X.; Zhan, J.; Sui, Y.W.; Qi, J.Q.; Wei, F.X.; Meng, Q.K.; He, Y.Z.; Ren, Y.J.; Zhan, Z.Z. Hierarchical NiS@CoS with controllable core–shell structure by two–step strategy for supercapacitor electrodes. *Adv. Mater. Interfaces* **2019**, *7*, 1901618. [CrossRef]
21. Iqbal, M.Z.; Khan, J. Optimization of cobalt-manganese binary sulfide for high performance supercapattery devices. *Electrochim. Acta* **2021**, *368*, 137529. [CrossRef]
22. Zardkhoshoui, A.M.; Ameri, B.; Davarani, S.S.H. alpha-MnS@Co_3S_4 hollow nanospheres assembled from nanosheets for hybrid supercapacitors. *Chem. Eng. J.* **2021**, *422*, 129953. [CrossRef]
23. Li, F.Z.; Zhen, C.; Dan, Z.; Sun, A.K.; Shi, P.; Liang, J.; He, Q.G. Neoteric hollow tubular MnS/Co_3S_4 hybrids as high-performance electrode materials for supercapacitors. *Electrochim. Acta* **2021**, *390*, 138893.
24. Zhao, Y.; Shi, Z.; Li, H.; Wang, C.A. Designing pinecone-like and hierarchical manganese cobalt sulfides for advanced supercapacitor electrodes. *J. Mater. Chem. A* **2018**, *6*, 12782–12793. [CrossRef]
25. Liu, H.M.; Li, Z.; Yao, Z.X.; Liu, Y.S.; Zhang, Q.F.; Sun, Y.J.; Li, Z. Designed MnS/Co_9S_8 micro-flowers composites with serrate edges as high-performance electrodes for asymmetric supercapacitor. *J. Colloid Interf. Sci.* **2019**, *551*, 119–129. [CrossRef] [PubMed]
26. Zhang, X.; Shi, C.; Guo, X.; Kong, R.M.; Qu, F.L. A $MnCo_2S_4$ nanowire array as an earth-abundant electrocatalyst for an efficient oxygen evolution reaction under alkaline conditions. *J. Mater. Chem. A* **2017**, *5*, 17211–17215. [CrossRef]
27. Saravanakumar, B.; Jayaseelan, S.S.; Seo, M.K.; Kim, H.Y.; Kim, B.S. $NiCo_2S_4$ nanosheet-decorated 3D, porous Ni film@Ni wire electrode materials for all solid-state asymmetric supercapacitor applications. *Nanoscale* **2017**, *9*, 18819–18834. [CrossRef]
28. Soonmin, H. Recent advances in the growth and characterizations of SILAR-deposited thin films. *Appl. Sci.* **2022**, *12*, 8184. [CrossRef]
29. Bagwade, P.P.; Malavekar, D.B.; Ubale, S.B.; Ghogare, T.T.; Bulakhe, R.N.; In, I.; Patil, U.M.; Lokhande, C.D. Characterization of Dy_2S_3 thin films deposited by successive ionic layer adsorption and reaction (SILAR) method. *Solid State Sci.* **2021**, *119*, 106693. [CrossRef]
30. Khot, S.D.; Malavekar, D.B.; Nikam, R.P.; Ubale, S.B.; Bagwade, P.P.; Patil, D.J.; Lokhande, V.C.; Lokhande, C.D. SILAR synthesized dysprosium selenide (Dy_2Se_3) thin films for hybrid electrochemical capacitors. *Synth. Met.* **2022**, *287*, 117075. [CrossRef]
31. Katkar, P.K.; Padalkar, N.S.; Padalkar, N.S.; Jeon, J.H.; Sheikh, Z.A.; Jerng, S.K.; Na, H.R.; Lee, S.; Chun, S.H. Development of amorphous Fe-doped nickel-cobalt phosphate (FexNiCo(PO_4)(2)) nanostructure for enhanced performance of solid-state asymmetric supercapacitors. *Int. J. Energy Res.* **2022**, *46*, 12039–12056. [CrossRef]
32. Patil, V.V.; Pujari, S.S.; Bhosale, S.B.; Kumbhar, S.S.; Parale, V.G.; Gunjakar, J.L.; Park, H.-H.; Lokhande, C.D.; Mali, M.G.; Mhamane, D.S.; et al. Hydrous and amorphous cobalt phosphate thin-film electrodes synthesized by the SILAR method for high-performing flexible hybrid energy storage devices. *Energy Fuels* **2022**, *36*, 12791–12806. [CrossRef]
33. Patil, A.S.; Patil, M.D.; Lohar, G.M.; Jadhav, S.T.; Fulari, V.J. Supercapacitive properties of CuO thin films using modified SILAR method. *Ionics* **2017**, *23*, 1259–1266. [CrossRef]
34. ElZein, B.; Abulikemu, M.; Barham, A.S.; Jabbour, G.E. In situ growth of PbS nanoparticles without organic linker on ZnO nanostructures via successive ionic layer adsorption and reaction (SILAR). *Coatings* **2022**, *12*, 1486. [CrossRef]
35. Seong, C.; Mane, P.; Bae, H.; Lee, S.; Kang, S.H.; Ryu, S.W.; Ha, J.S. Simple fabrication of BiVO4 thin films synthesized by modified SILAR method: Effect of film thickness. *J. Electrochem. Soc.* **2022**, *169*, 016501. [CrossRef]
36. Patil, D.J.; Malavekar, D.B.; Lokhande, C.D. Binder-free synthesis of mesoporous nickel tungstate for aqueous asymmetric supercapacitor applications: Effect of film thickness. *Energy Technol.* **2022**, *10*, 2600295. [CrossRef]
37. Admuthe, A.; Kumbhar, S.S.; Chougule, S.K.; Padasare, G.N.; Tonape, M.M. Synthesis and characterization of MnS thin film at room temperature for supercapacitor application. *Macromol. Symp.* **2020**, *392*, 2000186. [CrossRef]
38. Anish, R.N.; Sandhyarani, N. SILAR deposited nickel sulphide-nickel hydroxide nanocomposite for high performance asymmetric supercapacitor. *Electrochim. Acta.* **2020**, *356*, 136844.
39. Xu, J.; Xiang, C.L.; Fang, S.W.; Zhu, L.P.; Xu, F.; Sun, L.X.; Zou, Y.J.; Zhang, J. Template strategy to synthesize porous Mn-Co-S nanospheres electrode for high-performance supercapacitors. *Energy Storage* **2021**, *44*, 103267. [CrossRef]
40. Li, X.; Li, Q.; Wu, Y.; Rui, M.C.; Zeng, H.B. Two-dimensional, porous nickel-cobalt sulfide for high-performance asymmetric supercapacitors. *ACS Appl. Mater. Interfaces* **2016**, *8*, 22997–23005. [CrossRef]
41. Zhang, H.; Guan, B.; Gu, J.; Li, Y.; Ma, C.; Zhao, J.; Wang, T.Y.; Cheng, C.J. One-step synthesis of nickel cobalt sulphides particles: Tuning the composition for high performance supercapacitors. *RSC Adv.* **2016**, *6*, 58916–58924. [CrossRef]
42. Liu, H.; Guo, Z.; Wang, X.; Hao, J.; Lian, J.S. CuS/MnS composite hexagonal nanosheet clusters: Synthesis and enhanced pseudocapacitive properties. *Electrochem. Acta* **2018**, *271*, 425–432. [CrossRef]
43. Liu, S.; Jun, S.C. Hierarchical manganese cobalt sulfide core-shell nanostructures for high-performance asymmetric supercapacitors. *J. Power Sources* **2017**, *342*, 629–637. [CrossRef]
44. Iqbal, M.Z.; Zakar, S.; Haider, S.S.; Afzal, A.M.; Iqbal, M.J.; Kamran, M.A.; Numan, A. Electrodeposited CuMnS and CoMnS electrodes for high performance asymmetric supercapacitor devices. *Ceram. Int.* **2020**, *46*, 21343–21350. [CrossRef]
45. Lee, D.; Xia, Q.X.; Mane, R.S.; Yun, J.M.; Kim, K.H. Direct successive ionic layer adsorption and reaction (SILAR) synthesis of nickel and cobalt hydroxide composites for supercapacitor applications. *J. Alloys Compd.* **2017**, *722*, 809–817. [CrossRef]

46. Ubale, S.B.; Kale, S.B.; Mane, V.J.; Yun, J.M.; Kim, K.H. SILAR synthesized nanostructured ytterbium sulfide thin film electrodes for symmetric supercapacitors. *J. Solid State Electrochem.* **2021**, *25*, 1753–1764. [CrossRef]
47. Shinde, S.K.; Ramesh, S.; Yadav, H.M. Novel approach to synthesize $NiCo_2S_4$ composite for high performance supercapacitor application with different molar ratio of Ni and Co. *Sci. Rep.* **2019**, *9*, 13717. [CrossRef]
48. Raut, S.S.; Dhobale, J.A.; Sankapal, B.R. SILAR deposited Bi_2S_3 thin film towards electrochemical supercapacitor. *Phys.-Low-Dimens. Syst. Nanostruct.* **2017**, *87*, 209–212. [CrossRef]

Disclaimer/Publisher's Note: The statements, opinions and data contained in all publications are solely those of the individual author(s) and contributor(s) and not of MDPI and/or the editor(s). MDPI and/or the editor(s) disclaim responsibility for any injury to people or property resulting from any ideas, methods, instructions or products referred to in the content.